Geoscience Letters

RESEARCH LETTER

Open Access

Influence of El Niño–Southern Oscillation on moist static energy transport

Chae-Eun Hong[1], Dajeong Jeong[1], Ije Hur[1] and Changhyun Yoo[1*]

Abstract

This study investigates how El Niño–Southern Oscillation (ENSO) modulates the poleward transport of moist static energy (MSE) in the Northern Hemisphere winter. When an ENSO index increases by its one standard deviation, the MSE transport is enhanced by approximately 6% in the tropics (0°–15°N) and by 5% in the poleward of 40°N, while it is decreased by approximately 6–10% in 15°–40°N. The transport anomaly is mainly driven by changes in the mean meridional circulation associated with ENSO, with dry static energy transport being dominant over latent energy transport. In the extratropics, contributions from stationary and transient eddies are large, but tend to cancel each other out. The mean meridional transport anomaly is primarily explained by changes in the circulation, not by changes in the MSE. This contrast with the stationary transport anomaly, which consists of both circulation-driven and energy-driven changes. The transient dry static energy transport is the only component that follows the flux–gradient relationship. The study underscores the importance of changes in atmospheric circulation, rather than just energy itself, in shaping how energy is transported across latitudes during ENSO events.

Keywords Moist static energy, Meridional energy transport, El Niño–Southern Oscillation, Interannual variation

Introduction

The meridional transport of moist static energy (MSE) plays an important role in maintaining Earth's energy balance (Alexeev et al. 2005; Armour et al. 2019; Held and Soden 2006; Trenberth and Caron 2001; Trenberth and Stepaniak 2003b; Zelinka and Hartmann 2012). The MSE transport is dynamically determined by the meridional wind and the MSE itself. The resulting climatology of the MSE transport shows a smooth structure, with maximum poleward transport at midlatitudes (Hartmann 2016; Peixoto and Oort 1992). Energetically, climatological MSE transport must balance the energy surplus in the tropics and the deficit at high latitudes to maintain overall energy balance. This means that the time-averaged structure of the meridional MSE transport is determined by the energy exchanges at the top and bottom boundaries of the atmosphere. Additionally, the climatological MSE transport can be described diffusively, driven by the gradient of the climatological mean MSE. From this perspective, a gradient in the climatological MSE must result in a downgradient flux of the MSE (Armour et al. 2019).

In a warmer climate, an increase in the poleward MSE transport is anticipated based on the flux–gradient relationship (Held and Soden 2006; Merlis 2014; North 1975). This expectation arises from the Clausius–Clapeyron relation for constant relative humidity, which suggests that humidity increases more rapidly in the tropics than in other regions. Consistent with this diffusive perspective, climate models generally project an increase in poleward MSE transport (Armour et al. 2019; Held and Soden 2006; Hwang and Frierson 2010). However, recent evidence suggests that the MSE transport trend in recent decades does not fully align with the diffusive perspective (Clark et al. 2022). Instead, the dynamical perspective may offer a better framework for understanding the temporal variability in MSE transport. This is because, at any given moment, the MSE transport is likely to be driven

*Correspondence:
Changhyun Yoo
cyoo@ewha.ac.kr
[1] Department of Climate and Energy Systems Engineering, Ewha Womans University, Seoul, South Korea

Springer Open

© The Author(s) 2025. **Open Access** This article is licensed under a Creative Commons Attribution 4.0 International License, which permits use, sharing, adaptation, distribution and reproduction in any medium or format, as long as you give appropriate credit to the original author(s) and the source, provide a link to the Creative Commons licence, and indicate if changes were made. The images or other third party material in this article are included in the article's Creative Commons licence, unless indicated otherwise in a credit line to the material. If material is not included in the article's Creative Commons licence and your intended use is not permitted by statutory regulation or exceeds the permitted use, you will need to obtain permission directly from the copyright holder. To view a copy of this licence, visit http://creativecommons.org/licenses/by/4.0/.

dynamically by the circulation rather than diffusively by the MSE itself. This is especially true as the time scale of interest becomes shorter.

In this study, we use the El Niño–Southern Oscillation (ENSO) as a specific example to investigate how MSE transport changes on an interannual time scale. We choose ENSO because of its dominance in interannual time scale. Furthermore, we have a solid understanding of its effects on global temperature and precipitation (Lyon and Barnston 2005; Seager et al. 2005; Trenberth 1998), circulations such as the Hadley circulation (Guo and Li 2016; Oort and Yienger 1996; Sun and Zhou 2014), and stationary waves (Hoskins and Karoly 1981; Seager et al. 2010; Trenberth 1998). During El Niño, the central and eastern tropical Pacific becomes anomalously warmer, enhancing convection and thus latent heating in the equatorial upper troposphere (Cai et al. 2014; Sullivan et al. 2019). This enhanced heating strengthens the Hadley circulation (Quan et al. 2004) and amplifies stationary waves, particularly over the Pacific Ocean (Seager et al. 2010). As a result, poleward MSE transport is expected to increase in both the tropics and extratropics. However, the relative contributions of the zonal mean circulation versus eddies to these transport changes remain unclear. Also, the role of the MSE itself in driving these transport changes warrants further investigation.

Here, we examine the variability of MSE transport on interannual timescales in response to ENSO. The contribution of dry static energy (DSE) and latent energy (LE) were assessed, along with the roles of mean meridional circulation (MMC) and eddies. Additionally, we further decomposed the transport variability into climatological and anomaly components to separate circulation-driven, energy-driven, and interaction effects.

Data and methods

Data

We used the fifth-generation European Centre for Medium-Range Weather Forecasts Reanalysis (ERA5) dataset, covering the period from 1979 to 2020 (Hersbach et al. 2020). Five 6-hourly variables—meridional wind, temperature, geopotential, specific humidity, and surface pressure—were obtained from this dataset and averaged into daily means. The data were then bilinearly interpolated from the original 0.25°×0.25° resolution to a 1.25°×1.25° resolution. Additionally, we used the Japanese 55-year Reanalysis (JRA-55) dataset for the same period (Kobayashi et al. 2015) to verify the robustness of our results across different datasets.

To represent the ENSO state, we used the Ocean Niño Index (ONI) provided by the National Oceanic and Atmospheric Administration (NOAA 2019a). This index is constructed using the 3-month running averaged sea surface temperature (SST) anomalies in the Niño 3.4 region (5°N–5°S, 120°W–170°W) of the Extended Reconstructed SST version 5 dataset (Huang et al. 2017; NOAA 2019b). During the analysis period (1979–2020), we identified 14 El Niño events and 13 La Niña events, resulting in a total of 27 ENSO events for this study.

Moist static energy transport

MSE consists of the DSE and LE, and can be expressed as:

$$\mathrm{MSE} = \underbrace{gz + c_p T}_{DSE} + \underbrace{Lq}_{LE}, \tag{1}$$

where z represents the geopotential height, T is temperature, and q is the specific humidity, g denotes the gravitational constant, c_p denotes the specific heat of air, and L indicates the latent heat of vaporization. The zonally averaged MSE transport ($\widetilde{MSE}$) on an isobaric surface can be defined by:

$$\widetilde{MSE}(t,p,\phi) = [v(\mathrm{MSE})], \tag{2}$$

where the square brackets represent the zonal mean. Then $\widetilde{MSE}$ is a function of time (t), pressure (p), and latitude (ϕ). By integrating $\widetilde{MSE}$ vertically from 1000 to 1 hPa, the meridional MSE transport can be expressed as:

$$\langle \widetilde{MSE}(t,\phi) \rangle = \frac{2\pi a \cos\phi}{g} \int_{1000\mathrm{hPa}}^{1\mathrm{hPa}} [v(\mathrm{MSE})] dp, \tag{3}$$

where the angle brackets indicate the vertical integral, and a represents the Earth's radius. The total transport can be separated into the components of the MMC and the eddies. The eddies are further categorized into stationary and transient (Peixoto and Oort 1992). The decomposition into these components (i.e., MMC, stationary eddies, and transient eddies) is provided in Eq. (S1) in the Supporting Information. Throughout the study, the statistical significance is evaluated using a two-tailed t-test with a 5% significance level.

Results

Changes in the MSE transport

The winter mean MSE transport is northward across all latitudes in the Northern Hemisphere (black line in Fig. 1a), with varying contributions from the MMC, stationary, and transient eddy components (colored lines in Fig. 1a). The climatological MSE transport and its decompositions are consistent with reports from previous studies (Armour et al. 2019; Clark et al. 2022; Seager et al. 2005; Trenberth and Stepaniak 2003a). Similar results were obtained when the JRA55 dataset was used (Fig. S1). Specifically, the MSE transport by the MMC is poleward

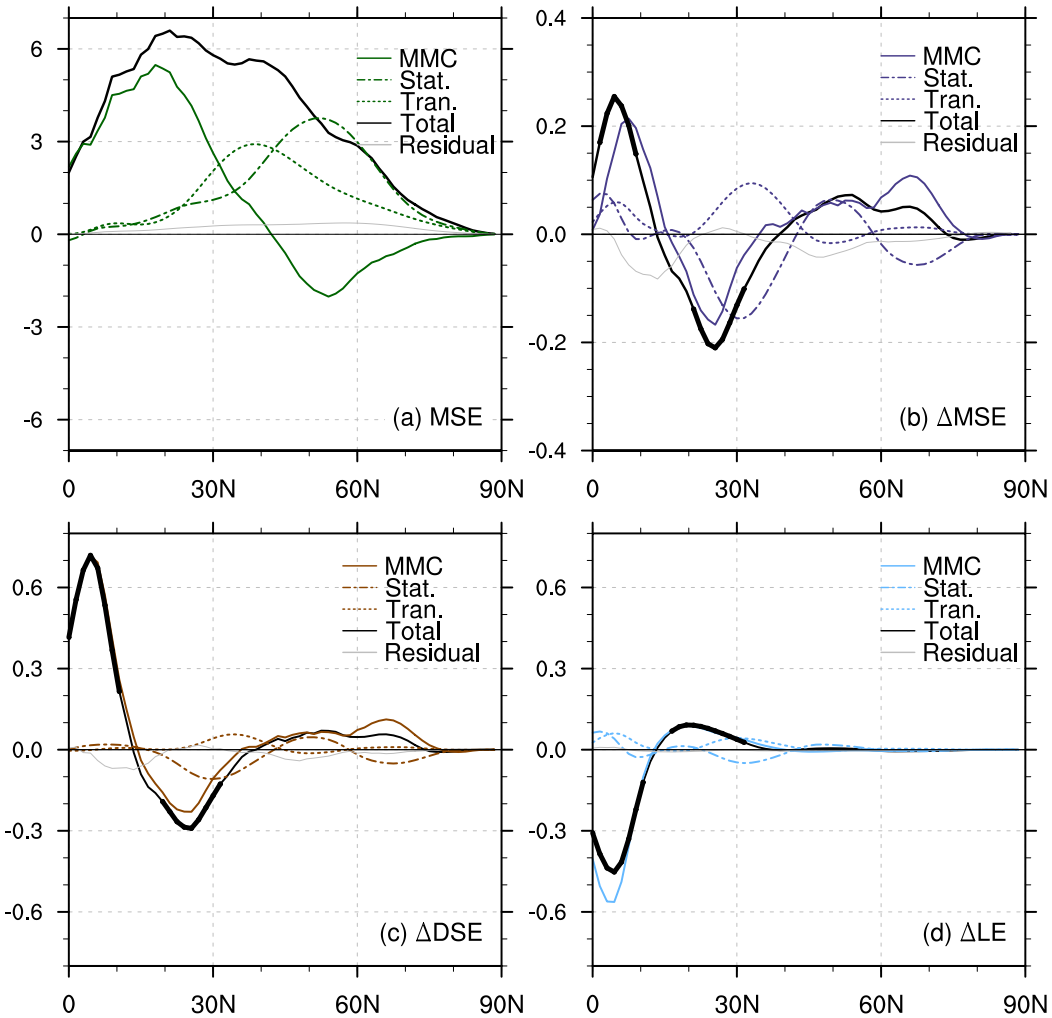


Fig. 1 **a** The DJF climatology of the northward transport of MSE by MMC (colored solid), stationary eddies (dash-dotted), transient eddies (dotted), total transport (black solid), and residual (gray solid). Regression of the northward flux of **b** MSE, **c** DSE, and **d** LE against the ONI during DJF from 1979 to 2020. The total transport is further divided into MMC and the eddy contributions. The transport unit is 10^{15} W. Bold black lines indicate statistical significance at the 95% confidence level

at low latitudes (0°–30°N) with a maximum amplitude of 5 PW (colored solid line in Fig. 1a). In the extratropics, the MMC contribution shifts to equatorward energy transport, with a magnitude of approximately 2 PW. This is due to the Hadley and Ferrel cells, which have poleward and equatorward branches, respectively, in the upper troposphere. In contrast, the stationary and transient eddies are the dominant drivers of the poleward MSE transport in the extratropics, with maxima of about 3–4 PW (dash-dotted and dotted lines in Fig. 1a). However, their contribution is smaller at low latitudes. Unlike the MMC, the climatological eddy transports show poleward energy transport across all latitudes.

In response to an increase in the ONI, MSE transport strengthens in the equatorial region (0°–15°N) and north of 40°N, while it weakens in the region between 15°N and 40°N (black line in Fig. 1b), compared to the climatological mean of MSE transport (black line in Fig. 1a). The MSE transport anomaly in response to one standard deviation change in the ONI ranges from approximately 6–10% of its December–January–February (DJF) climatology. A two-tailed t-test at the 5% level confirms that these anomalies are statistically significant across large portions of the equatorial and midlatitude regions (bold black lines in Fig. 1). We note that the transport anomaly was generally inconsistent with the MSE anomaly associated with the ENSO (Fig. S2). For example, a negative MSE gradient (dotted line in Fig. S2a) is observed near 30°N, where the transport anomaly is equatorward (black solid line in Fig. 1a). This is plausible because MSE is not

a conserved quantity; it can be generated or lost through processes such as diabatic heating, especially those associated with ENSO. This is particularly relevant on time scales where atmospheric dynamics dominate the variability of MSE transport. The MSE transport anomaly is contributed predominantly by the MMC (see the match between the black and the colored solid lines in Fig. 1b), while substantial cancellation occurs between the MSE transport by stationary and transient eddies. The MMC component exhibits the largest anomaly in the tropics (colored solid line in Fig. 1b). In contrast, the magnitudes of the MMC and the two eddies are comparable in the extratropics (dash-dotted and dotted lines in Fig. 1b).

Our analysis revealed that DSE transport plays a crucial role in the MSE transport associated with ENSO. To identify the components contributing to the variability in MSE transport, we first decomposed the MSE into DSE and LE (Fig. 1c–d). Overall, the MSE transport anomaly (black line in Fig. 1b) roughly follows the structure of DSE transport (black line in Fig. 1c). Further decomposing the DSE into geopotential energy (GE) and sensible energy (SE) transports, we find that the MMC transport anomaly is primarily explained by the GE, while the eddy transport anomaly is largely influenced by the SE (Fig. S3). This will be further discussed in the following subsections. Compared to the MSE transport, the LE transport anomalies (black lines in Fig. 1d) show slightly different patterns or even opposite signs. For LE, the MSE transport in the tropics is similarly dominated by the MMC, with relatively small contributions from the eddies (Fig. 1d). However, in the extratropics, similar to the DSE transport, the LE transport becomes substantially dominated by the eddies. Nevertheless, we will show that the LE and SE transports by eddies are subject to cancellation between stationary and transient eddies, resulting in the MMC being the main driver of the observed variability.

Dominant contribution by circulation-driven changes

In the previous subsection, we established that the ENSO-induced changes in MSE transport in the tropics are mainly driven by the DSE transport of the MMC, particularly by the GE transport of the MMC. In contrast, the MSE transport anomaly in the extratropics is strongly influenced by the eddy contributions of the SE and LE transport, as well as the MMC of the DSE transport. We now examine how the ENSO drives these changes by decomposing each variable into its climatology and the deviation from the climatology (Eqs. S2–S3). Additionally, the MMC and stationary eddy transport terms were further broken down into contributions from circulation changes, energy changes, and the interaction between these two factors (Eqs. S4–S5).

We find that variability in MSE transport through the MMC is primarily driven by changes in the Hadley circulation. During El Niño events, the anomalous warming in the central and eastern tropical Pacific leads to increased deep convection and diabatic heating in the equatorial upper troposphere. This heating increases the meridional temperature gradient, which strengthens the Hadley circulation via the thermal wind balance. Additionally, changes in the subtropical jets influence transient eddy propagation and momentum fluxes, further modulating the MMC (Seager et al. 2003). Accordingly, as the ONI increases, the meridional wind shows stronger poleward in the upper level and enhanced equatorward motions near the surface, respectively (Fig. 2a). This strengthened Hadley cell pattern is evident across all MSE components in the pressure–latitude space (Fig. 2b–c). For the DSE transport, the resemblance with the MMC pattern is pronounced throughout the Northern Hemisphere (Fig. 2b). Since geopotential increases with height, the DSE transport anomaly linked to the MMC peaks in the upper troposphere (Fig. 2b). In the lower troposphere, however, the DSE transport anomaly is smaller despite higher values near the surface, due to temperature and meridional wind structures. In contrast, the LE transport exhibits a pronounced negative anomaly at the base of the Hadley cell, where moisture is more concentrated near the surface (Fig. 2c). This vertical structure of DSE and LE transport anomalies implies that El Niño-induced upper-level DSE convergence leads to warming in the tropical and midlatitude upper troposphere, while LE convergence near the equator enhances convection and precipitation. Conversely, LE divergence in the subtropics can suppress convection, leading to reduced precipitation in those regions.

For all MSE components, the ENSO-related changes in the meridional wind are the primary drivers of the MSE transport anomaly through the MMC. In other words, variations in the MSE themselves contribute minimally to the transport anomalies. This is clearly demonstrated when the terms are broken down, as shown in Eq. (S4). Here, the circulation-driven term corresponds to the transport of the climatological zonal mean temperature by the ENSO-related anomalous circulation, while the energy-driven term represents the transport of the ENSO-related temperature anomalies by the climatological circulation. Figure 2d–e reveals that the vertically integrated MMC transport can be almost completely reconstructed by the circulation-driven term (1st), with only minor contributions from the energy-driven term (2nd) in the tropics. This holds true for both the DSE and LE, and the interaction term (3rd) is negligible.

We now focus on the changes in MSE transport driven by the stationary eddy. During El Niño, enhanced

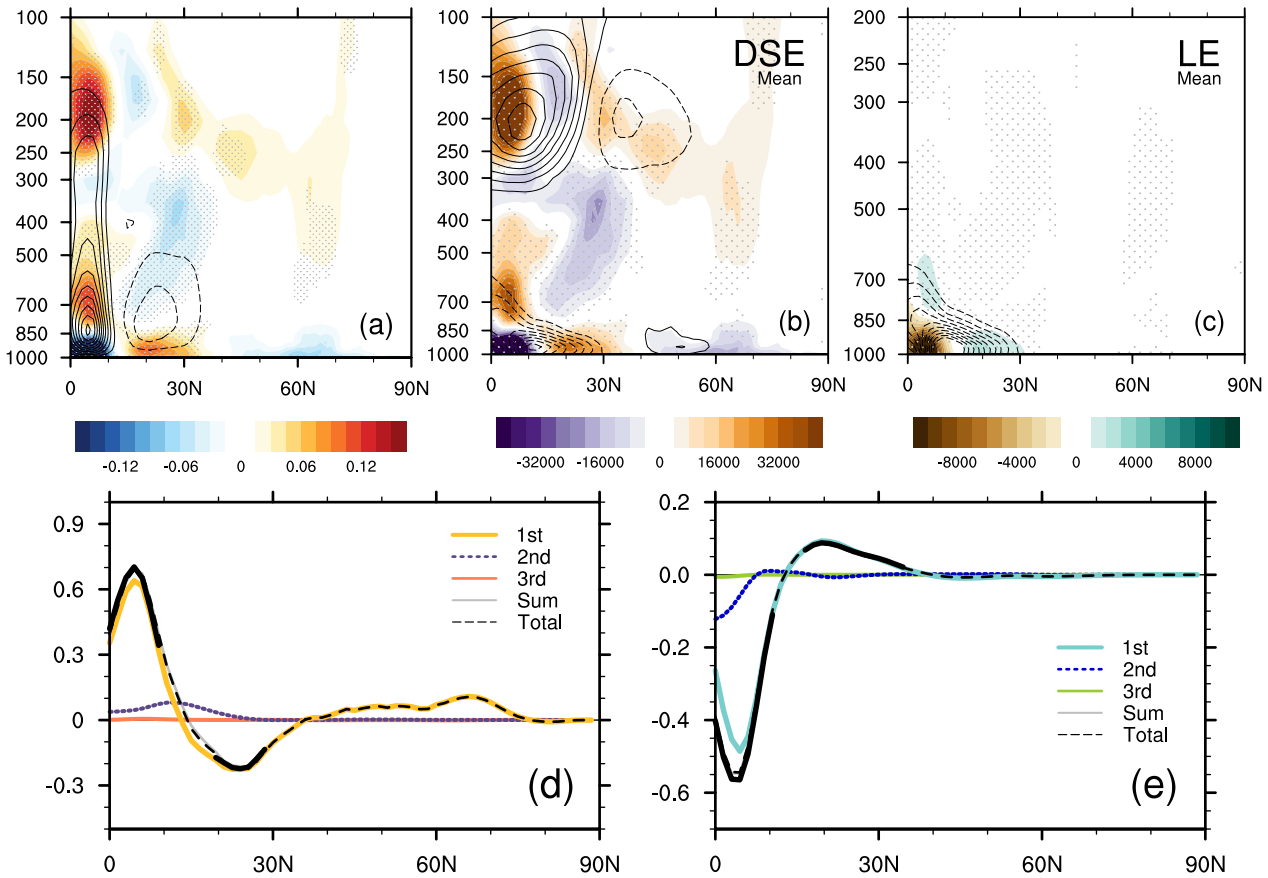


Fig. 2 Shading represents the regression of zonally averaged **a** meridional wind, **b** northward fluxes of DSE, and **c** LE onto ONI during DJF from 1979 to 2020 by MMC. Black contours indicate the **a** stream function regressed onto ONI, DJF climatological fluxes of **b** DSE and **c** LE. Regression of vertically averaged northward flux of **d** DSE onto ONI (black dashed), with terms divided into contributions from the circulation-driven term (1st), the energy-driven term (2nd), and the interaction term between the two (3rd). **e** Same as **d** but for LE. Gray dots and bold black lines indicate areas of statistical significance at the 95% confidence level

convective heating in the equatorial central Pacific alters the upper tropospheric divergence and enhances the generation of Rossby wave trains that propagate into the extratropics. This process induces a positive Pacific/North American (PNA) pattern in the Northern Hemisphere (Barnston and Livezey 1987; Johnson and Feldstein 2010; Wallace and Gutzler 1981). This positive PNA-like pattern (shading in Fig. S5b) is associated with a deepened Aleutian low, indicating an eastward shift of the climatological trough in the North Pacific (contours in Fig. S5b). A decrease in the MSE transport was observed from the stationary eddy component, except between 40°N and 50°N (dash-dotted line in Fig. 1b). This is mainly due to decreases in the SE and LE components, while the GE component shows only a minor change (black line in Fig. S4c). Similar to the MMC transport anomaly, changes in the LE transports are concentrated near the surface. In contrast, the DSE transport is distributed throughout the troposphere (shading in Fig. 3a–b). These anomalous patterns are broadly consistent with precipitation and geopotential height composites during El Niño events (e.g., deeper Aleutian low and North Pacific trough shift), supporting the connection between our MSE analyses and canonical ENSO teleconnection patterns over the North Pacific and North America (Lau and Nath 1994; Straus and Shukla 2002).

The reduction in stationary eddy transport is attributed to strong cancellations between the circulation-driven (1st) and energy-driven (2nd) terms (Fig. 3c–d; see also Eq. S5). The interaction term (i.e., the 3rd term in Eq. S5) contributes minimally to the DSE transport anomalies but plays a relatively more important role in the LE transport. Similarly, decomposing the DSE into GE and SE reveals that the variability of DSE is predominantly driven by SE, while the contribution of GE remains negligible (black dashed line in Fig. S4c–d). This result is consistent with the geostrophic balance, which ensures that the geopotential and the meridional wind are orthogonal

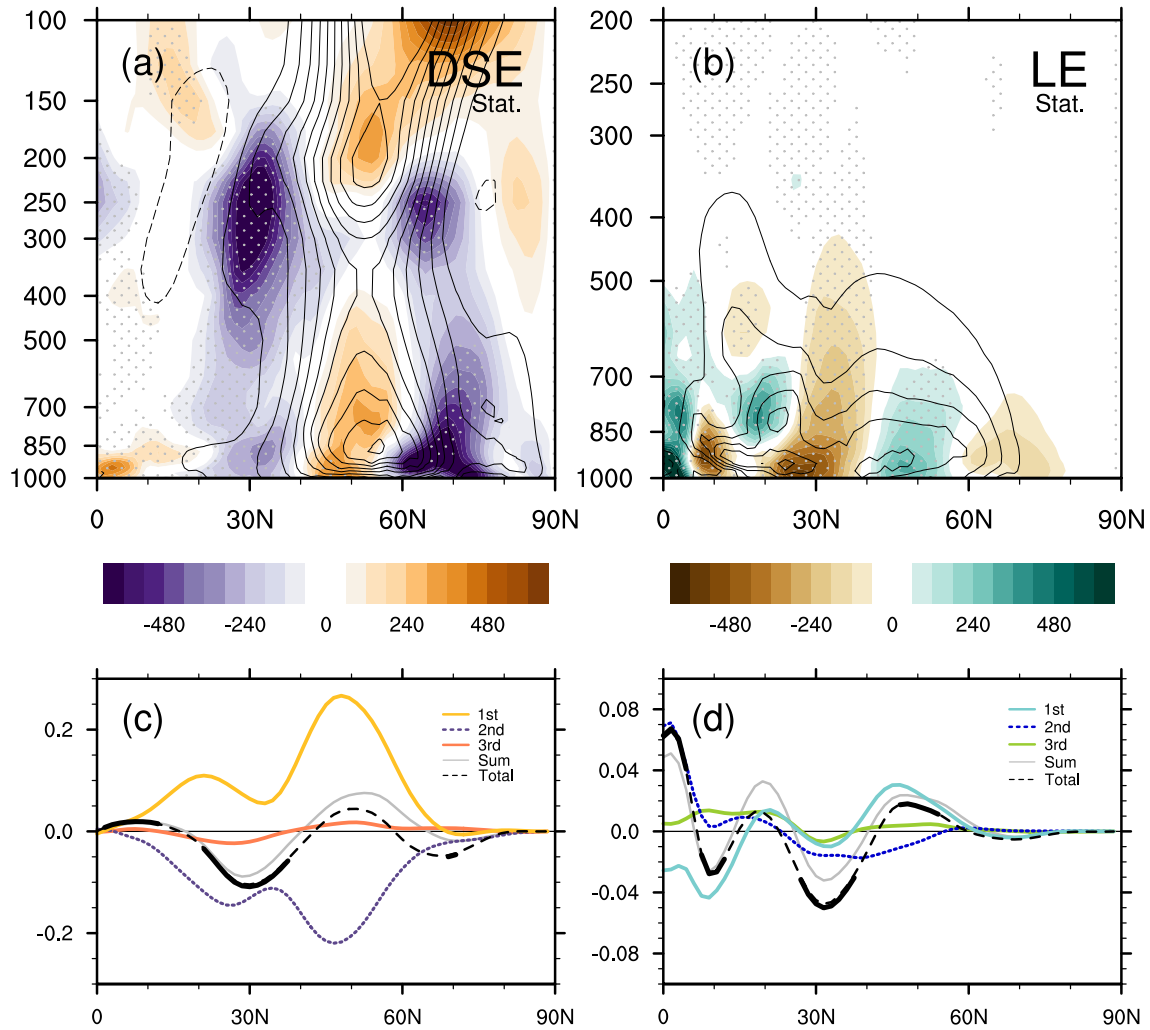


Fig. 3 Shading represents the regression of zonally averaged northward fluxes of **a** DSE and **b** LE onto ONI during DJF from 1979 to 2020 by stationary eddies. Black contours indicate the DJF climatological energy fluxes. Regression of vertically averaged northward flux of **c** DSE onto ONI (black dashed), with terms divided into contributions from the circulation-driven term (1st), the energy-driven term (2nd), and the interaction term between the two (3rd). **d** Same as **c** but for LE. Gray dots and bold black lines indicate areas of statistical significance at the 95% confidence level

to each other (Fig. S5a–b). As the geostrophic meridional wind is proportional to the zonal gradient of geopotential, this orthogonality reduces the covariance between the two, resulting in a negligible stationary eddy transport of GE. Therefore, for DSE, the negative transport anomaly by the energy-driven term makes a relatively stronger contribution than the positive circulation-driven term, except between 40°N and 50°N (Fig. 3c). The negative energy-driven term results from the stationary DSE anomaly (shading in Fig. S5b) negatively projecting onto the climatological stationary meridional wind (contours in Fig. S5a). In contrast, the positive circulation-driven term arises from the stationary circulation anomaly (shading in Fig. S5a) positively projecting onto the climatological stationary DSE (contours in Fig. S5b). For LE, all terms contribute to the total anomaly (Fig. 3d) due to interactions between moisture and circulation anomalies associated with the ENSO (Fig. S5a, c).

Finally, the changes in the transient DSE transport associated with the ENSO exhibit poleward anomalies in the subtropics (~30°N) and subpolar regions (~65°N), along with a negative anomaly around 25°N and 50°N (Fig. 4a, c). The variation in DSE transport by transient eddies, similar to stationary eddies, is also largely influenced by the SE. This pattern aligns with the gradient of the zonal mean DSE anomaly induced by the ENSO (Fig.

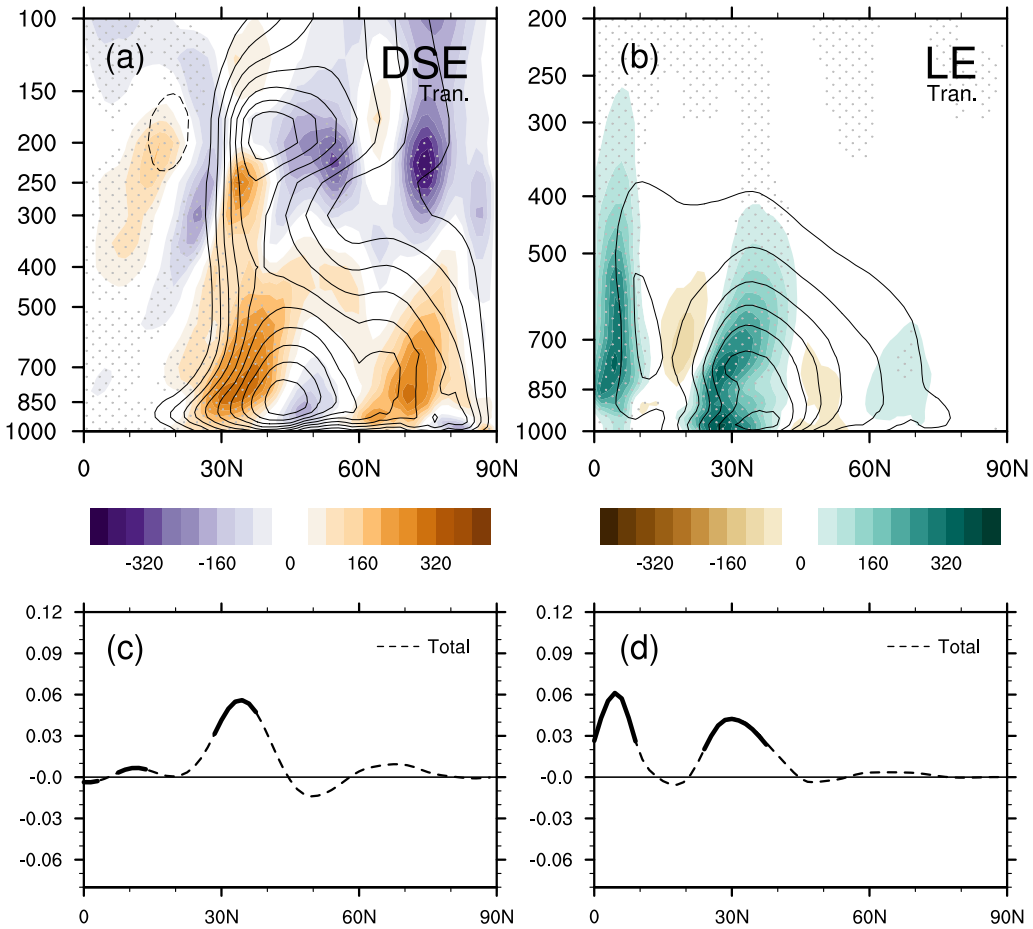


Fig. 4 Shading represents the regression of zonally averaged northward fluxes of **a** DSE and **b** LE onto ONI during DJF from 1979 to 2020 by transient eddies. Black contours indicate the DJF climatological energy fluxes. Regression of vertically averaged northward flux of **c** DSE onto ONI (black dashed). **d** Same as **c** but for LE. Gray dots and bold black lines indicate areas of statistical significance at the 95% confidence level

S6a). For example, the increased DSE gradient, resulting from upper tropospheric warming near the equator, enhances the transient eddy DSE flux around 30°N. Additionally, the warm anomaly centered at 60°N reduces the DSE flux near 50°N while increasing it near 65°N. These findings support the notion that a diffusive flux–gradient relationship can explain the transient DSE transport anomaly associated with the ENSO.

The transient LE transport exhibits anomalies similar to those of the transient DSE transport (Fig. 4b, d), with increases in LE transport corresponding to increases in SE transport and decreases in one corresponding to decreases in the other. However, a notable difference is the more pronounced LE transport anomaly in the equatorial region, likely due to the abundance of moisture in that area. The zonal mean moisture anomaly associated with the ENSO differs from that of the zonal mean temperature anomaly (Fig. S6b), indicating that the transient LE transport is more closely linked to the temperature gradient than to the moisture gradient. This is because, in the midlatitudes (around 30°N), the transient LE transport anomalies intensify when baroclinic eddies, driven by temperature gradients, transport moisture poleward.

Conclusions and discussion

This study investigated how the MSE transport changes in response to the ENSO. During El Niño, the MSE transport increases in the tropics (0°–15°N) and poleward of 40°N, while it decreases between 15°N and 40°N. These transport anomalies are primarily driven by changes in circulation, particularly by the MMC, rather than by shifts in the MSE gradient associated with ENSO. The key findings are summarized below:

- The MSE transport anomalies are most pronounced in the tropics and at high latitudes, primarily driven by changes in the MMC. Contributions from the stationary and transient eddies are large in the

extratropics; however, a strong cancellation occurs between these two contributions.

- The structure of the MMC associated with ENSO is evident across all MSE transport components. During El Niño, the DSE transport shows a positive anomaly in the equatorial region, driven by the enhanced poleward flow at the top of the Hadley cell, which primarily increases the poleward transport of GE in the upper levels of the tropics. In contrast, the LE transport exhibits a negative anomaly due to equatorward flow near the surface.
- During El Niño, reductions in the stationary DSE and LE transports are generally observed in the extratropics. This reduction results from strong cancellations between the circulation-driven and energy-driven terms. For DSE, the negative energy-driven term outweighs the positive circulation-driven term except between 40°N and 50°N. However, for LE, all terms contribute significantly due to interactions between moisture and circulation anomalies associated with ENSO.
- The transient transports effectively counterbalance the anomalies induced by the stationary DSE and LE transports. The transient DSE transport anomaly follows a diffusive flux–gradient relationship, while the transient LE transport does not. The similarity between the transient DSE and LE transport anomalies in the midlatitudes suggests that baroclinic eddies, influenced by baroclinicity, play an important role in the poleward transport of moisture.

These results extend previous studies by demonstrating that the MSE transport anomalies associated with ENSO are primarily driven by circulation changes, rather than by MSE gradients. This highlights the dominant role of dynamical processes on interannual timescales. We also compared MSE transport patterns between eastern Pacific (EP) and central Pacific El Niños and found a closer resemblance to those associated with EP events. This is likely due to the typically stronger mean circulation response associated with EP El Niño episodes (Hong et al. 2023). In particular, the stronger upper-level Hadley circulation response during EP events plays a key role in shaping the vertical structure of DSE transport anomalies, although this response varies across ENSO types and years. While these differences do not affect the main conclusions of the study, they highlight the need for further investigation in future work. As in the NH, the MMC component in the Southern Hemisphere closely matches the total anomaly, with stationary and transient eddy components largely cancelling each other out (Fig. S7). The MSE anomaly in the Southern Hemisphere is roughly half the magnitude observed in the NH.

This study examined the relationship between MSE transport and ENSO, with a focus on identifying the key components driving transport variability. However, the temporal sequence of these components—specifically which elements lead or lag in energy transport variability—was not addressed. Future research incorporating lag analysis could offer a more detailed understanding of the stepwise evolution of MSE transport in response to ENSO phases. Such analysis would improve mechanistic insights into the drivers of energy transport variability and their interactions with large-scale climate phenomena.

A significant shift in atmospheric circulation patterns is projected: the Hadley cell is likely to expand in a warmer climate, with the Southern Hemisphere shifting by approximately 2° and the Northern Hemisphere by 1° relative to the 1920–1960 baseline according to CMIP5 and CMIP6 simulations under high-emission scenarios (Grise and Davis 2020; Grise et al. 2019; Hur et al. 2022). Despite this general trend, individual models show considerable variability in the magnitude of expansion. A key question for future research is how these different MMC responses might affect MSE transport. In addition, for such long-term changes, MSE transport is likely to be shaped by the flux–gradient relationship. Internal variability, such as ENSO, may also change under global warming. Some studies suggest increased amplitude and spatial extent of ENSO-related SST and precipitation variability, potentially affecting the dynamical component of MSE transport (Cai et al. 2021; Yan et al. 2020). While long-term changes may follow the flux–gradient relationship, accounting for shorter-timescale variability remains important for understanding and quantifying future MSE transport changes. Understanding changes in MSE transport is critical for accurately predicting regional climate impacts and for advancing our understanding of MSE transport dynamics.

Supplementary Information

The online version contains supplementary material available at https://doi.org/10.1186/s40562-025-00405-6.

Supplementary material 1.

Author contributions

C.H. conducted the analysis and prepared the figures. C.H. and C.Y. drafted the manuscript. D.J. and I.H. contributed to the calculations. All authors reviewed and approved the final manuscript.

Funding

This research was supported by the Korea Environmental Industry and Technology Institute through grant KEITI-2022003560001, the National Research Foundation of Korea through grant RS-2024–00333469, and the Specialized University Program for Confluence Analysis of Weather and Climate Data of the Korea Meteorological Institute.

Data availability

ERA5 reanalysis datasets are available from ECMWF https://cds.climate.copernicus.eu/datasets/reanalysis-era5-pressure-levels (Hersbach et al., 2020). JRA55 data are available at https://diasjp.net/en/ (Kobayashi et al., 2015). The ENSO index, Niño 3.4 data, is downloaded from the NOAA Earth System Research Laboratory https://psl.noaa.gov/data/timeseries/month/Nino3/ (Rayner et al., 2003).

Declarations

Competing interests

The authors declare no competing interests.

Received: 21 May 2025 Accepted: 20 July 2025
Published online: 01 August 2025

References

Alexeev VA, Langen PL, Bates JR (2005) Polar amplification of surface warming on an aquaplanet in "ghost forcing" experiments without sea ice feedbacks. Clim Dyn 24(7):655–666

Armour KC, Siler N, Donohoe A, Roe GH (2019) Meridional atmospheric heat transport constrained by energetics and mediated by large-scale diffusion. J Climate 32(12):3655–3680

Barnston AG, Livezey RE (1987) Classification, seasonality and persistence of low-frequency atmospheric circulation patterns. Mon Weather Rev 115(6):1083–1126

Cai W, Borlace S, Lengaigne M, van Rensch P, Collins M, Vecchi G, Timmermann A, Santoso A, McPhaden MJ, Wu L, England MH, Wang G, Guilyardi E, Jin F-F (2014) Increasing frequency of extreme El Niño events due to greenhouse warming. Nat Clim Chang 4(2):111–116

Cai W, Santoso A, Collins M, Dewitte B, Karamperidou C, Kug J-S, Lengaigne M, McPhaden MJ, Stuecker MF, Taschetto AS, Timmermann A, Wu L, Yeh S-W, Wang G, Ng B, Jia F, Yang Y, Ying J, Zheng X-T, Bayr T, Brown JR, Capotondi A, Cobb KM, Gan B, Geng T, Ham Y-G, Jin F-F, Jo H-S, Li X, Lin X, McGregor S, Park J-H, Stein K, Yang K, Zhang L, Zhong W (2021) Changing El niño-Southern oscillation in a warming climate. Nat Rev Earth Environ 2(9):628–644

Clark JP, Feldstein SB, Lee S (2022) Moist static energy transport trends in four global reanalyses: are they downgradient? Geophys Res Lett. https://doi.org/10.1029/2022GL098822

Grise KM, Davis SM (2020) Hadley cell expansion in CMIP6 models. Atmos Chem Phys 20(9):5249–5268

Grise KM, Davis SM, Simpson IR, Waugh DW, Fu Q, Allen RJ, Rosenlof KH, Ummenhofer CC, Karnauskas KB, Maycock AC, Quan X-W, Birner T, Staten PW (2019) Recent tropical expansion: natural variability or forced response?: J Climate 32(5):1551–1571

Guo Y-P, Li J-P (2016) Impact of ENSO events on the interannual variability of Hadley circulation extents in boreal winter. Adv Clim Chang Res 7(1):46–53

Hartmann DL (2016) Chapter 6–Atmospheric general circulation and climate: global physical climatology, 2nd edn. Elsevier, Amsterdam

Held IM, Soden BJ (2006) Robust responses of the hydrological cycle to global warming. J Climate 19(21):5686–5699

Hersbach H, Bell B, Berrisford P, Hirahara S, Horányi A, Muñoz-Sabater J, Nicolas J, Peubey C, Radu R, Schepers D, Simmons A, Soci C, Abdalla S, Abellan X, Balsamo G, Bechtold P, Biavati G, Bidlot J, Bonavita M, De Chiara G, Dahlgren P, Dee D, Diamantakis M, Dragani R, Flemming J, Forbes R, Fuentes M, Geer A, Haimberger L, Healy S, Hogan RJ, Hólm E, Janisková M, Keeley S, Laloyaux P, Lopez P, Lupu C, Radnoti G, De Rosnay P, Rozum I, Vamborg F, Villaume S, Thépaut J-N (2020) The ERA5 global reanalysis. Q J R Meteorol Soc 146(730):1999–2049

Hong Q, Feng J, Li J (2023) Modulation of the central Pacific El Niño on the relationship between the Hadley circulation and tropical SST. J Geophys Res Atmos 128(13):e2022JD038195

Hoskins BJ, Karoly DJ (1981) The steady linear response of a spherical atmosphere to thermal and orographic forcing. J Atmos Sci 38(6):1179–1196

Huang B, Thorne PW, Banzon VF, Boyer T, Chepurin G, Lawrimore JH, Menne MJ, Smith TM, Vose RS, Zhang H-M (2017) Extended reconstructed sea surface temperature, version 5 (ERSSTv5): upgrades, validations, and intercomparisons. J Climate 30(20):8179–8205

Hur I, Kim M, Kwak K, Sung HM, Byun Y-H, Song H, Yoo C (2022) Hadley circulation in the present and future climate simulations of the K-ACE model. Asia-Pac J Atmos Sci 58(3):353–363

Hwang Y-T, Frierson DMW (2010) Increasing atmospheric poleward energy transport with global warming. Geophy Res Lett 37:24

Johnson NC, Feldstein SB (2010) The continuum of North Pacific sea level pressure patterns: intraseasonal, interannual, and interdecadal variability. J Climate 23(4):851–867

Kobayashi S, Ota Y, Harada Y, Ebita A, Moriya M, Onoda H, Onogi K, Kamahori H, Kobayashi C, Endo H, Miyaoka K, Takahashi K (2015) The JRA-55 reanalysis: general specifications and basic characteristics. J Meteorol Soc Japan Ser II 93(1):5–48

Lau N, Nath MJ (1994) A modeling study of the relative roles of tropical and extratropical SST anomalies in the variability of the global atmosphere-ocean system. J Climate 7(8):1184–1207

Lyon B, Barnston AG (2005) ENSO and the spatial extent of interannual precipitation extremes in tropical land areas. J Climate 18(23):5095–5109

Merlis TM (2014) Interacting components of the top-of-atmosphere energy balance affect changes in regional surface temperature. Geophys Res Lett 41(20):7291–7297

NOAA (2019a) Cold and warm episodes by season, Volume 2023.

NOAA (2019b) Nino regions, Volume 2023.

North GR (1975) Theory of energy-balance climate models. J Atmos Sci 32(11):2033–2043

Oort AH, Yienger JJ (1996) Observed interannual variability in the Hadley circulation and its connection to ENSO. J Clim 9(11):2751–2767

Peixoto JP, Oort AH (1992) Physics of climate. American Institute of Physics, New York

Quan X-W, Diaz HF, Hoerling MP (2004) Change in the tropical Hadley cell since 1950. In: Diaz HF, Bradley RS (eds) The hadley circulation: present, past and future. Springer, Dordrecht, pp 85–120

Rayner NA, Parker DE, Horton EB, Folland CK, Alexander LV, Rowell DP, Kent EC, Kaplan A (2003) Global analyses of sea surface temperature, sea ice, and night marine air temperature since the late nineteenth century. J Geophys Res Atmos. https://doi.org/10.1029/2002JD002670

Seager R, Harnik N, Kushnir Y, Robinson W, Miller J (2003) Mechanisms of hemispherically symmetric climate variability. J Climate 16(18):2960–2978

Seager R, Harnik N, Robinson WA, Kushnir Y, Ting M, Huang H-P, Velez J (2005) Mechanisms of ENSO-forcing of hemispherically symmetric precipitation variability. Q J R Meteorol Soc 131(608):1501–1527

Seager R, Naik N, Ting M, Cane MA, Harnik N, Kushnir Y (2010) Adjustment of the atmospheric circulation to tropical Pacific SST anomalies: variability of transient eddy propagation in the Pacific-North America sector. Q J R Meteorol Soc 136(647):277–296

Straus DM, Shukla J (2002) Does ENSO force the PNA? J Climate 15(17):2340–2358

Sullivan SC, Schiro KA, Stubenrauch C, Gentine P (2019) The response of tropical organized convection to El Niño warming. J Geophys Res Atmos 124(15):8481–8500

Sun Y, Zhou T (2014) How does El Niño affect the interannual variability of the boreal summer Hadley circulation? J Clim 27(7):2622–2642

Trenberth KE (1998) Atmospheric moisture residence times and cycling: implications for rainfall rates and climate change. Clim Change 39(4):667–694

Trenberth KE, Caron JM (2001) Estimates of meridional atmosphere and ocean heat transports. J Climate 14(16):3433–3443

Trenberth KE, Stepaniak DP (2003a) Covariability of components of poleward atmospheric energy transports on seasonal and interannual timescales. J Climate 16(22):3691–3705

Trenberth KE, Stepaniak DP (2003b) Seamless poleward atmospheric energy transports and implications for the hadley circulation. J Clim 16(22):3706–3722

Wallace JM, Gutzler DS (1981) Teleconnections in the geopotential height field during the Northern Hemisphere winter. Mon Weather Rev 109(4):784–812

Yan Z, Wu B, Li T, Collins M, Clark R, Zhou T, Murphy J, Tan G (2020) Eastward shift and extension of ENSO-induced tropical precipitation anomalies under global warming. Sci Adv 6(2):eaax4177
Zelinka MD, Hartmann DL (2012) Climate feedbacks and their implications for poleward energy flux changes in a warming climate. J Climate 25(2):608–624

Publisher's Note

Springer Nature remains neutral with regard to jurisdictional claims in published maps and institutional affiliations.